An Interdigitated Non-Contact ECG Electrode for Impedance Compensation and Signal Restoration

Jeng-Hau Lin[1], Hao Liu[2], Chia-Hung Liu[3], Phillip Lam[1], Gung-Yu Pan[3], Hao Zhuang[1], Ilgweon Kang[1], Patrick P. Mercier[2], Chung-Kuan Cheng[1,2]

1. Dept. of Computer Science and Engineering, University of California, San Diego
2. Dept. of Electrical and Computer Engineering, University of California, San Diego
3. Dept. of Electronics Engineering, National Chiao Tung University

{jel252, hal7, chl437, plam, g1pan, zhuangh, igkang, pmercier, ckcheng}@ucsd.edu

***Abstract*—This paper presents a non-contact electrocardiogram (ECG) measurement platform that compensates for motion-induced impedance changes via interdigitated electrode channels in concert with software reconstruction algorithms. Specifically, the impedance of the non-contact electrode is non-invasively acquired in real-time by exploiting a custom electrode designed with two independent channels featuring independent transfer functions that are used to reconstruct motion-compensated ECG waveforms. The developed platform is validated on human subjects, illustrating up to a 76.3% improvement over conventional approaches, paving the path towards comfortable, convenient, and robust non-contact electrophysiological sensing.**

I. Introduction

Measurement of electrocardiograms (ECGs) in freely-behaving subjects is used to diagnose and monitor a wide variety of heart conditions. Unlike wet ECG electrodes, which are uncomfortable and necessitate long and inconvenient preparation times, non-contact ECG electrodes can be integrated directly into clothing and offers a convenient way to measure long-term ambulatory ECG. However, non-contact ECG systems suffer from poor transduction range and severe motion artifacts. While many prior publications have attempted to improve coupling range via modified layer structures [1] and materials [2], or have attempted to increase SNR by introducing active guards and shields [3, 4], there has been comparatively little work on addressing motion-artifacts caused by impedance variation of non-contact electrodes.

For example, while an analytical model of time-domain motion artifacts was derived in [5] that could in principal be used to attenuate artifacts, the model considered only a capacitive electrode model, and further did not propose a way to monitor this capacitance in real time. To address this, a signal-injection method was introduced in [6] that enables real-time measurement of electrode capacitance, though it was focused on addressing static-charge-based motion artifacts, and again only considered a capacitive electrode model. As an alternative approach, Yin et al. [7] and our group had proposed a two-channel capacitive ECG recovery method that could compute the electrode coupling capacitance, C_C, thereby enabling reconstruction of the underlying ECG prior to C_C-variation induced distortion [8]. Figure 1 and Eq. (1) show the theory of two-channel capacitive recovery method, where $V_s(t)$ is the ECG signal without being distorted by the varying capacitive divider, $Q(t)$ is the eletrostatic charge accumulated by resipration or motion, and $C_{p\{1,2\}}$ are shunt capacitors found at the input of the amplifier, which were designed to be different with each other to facilitate independent transfer functions.

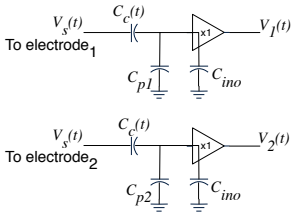

Figure 1. The model of two-channel capacitive recovery method for non-contact electrodes.

$$\begin{cases} V_1 = \frac{V_s(t)\cdot C_C(t)+Q(t)}{C_C(t)+C_{p1}} \\ V_2 = \frac{V_s(t)\cdot C_C(t)+Q(t)}{C_C(t)+C_{p2}} \end{cases} \quad (1)$$

Unfortunately, the electrode model employed in [5-8] was oversimplified for practical non-contact electrodes, as Gandhi et al. [9] have shown that commonly-employed dielectrics have finite resistivity. Thus, non-contact electrode models must at minimum include a resistor, R_e, parallel with the coupling capacitor, C_C. In fact, the resistance in many characterized dielectrics such as soldermask and cotton ranges from MΩ to GΩ, which may be smaller than the impedance of C_C in the 0.5-150 Hz ECG frequency band, and thus may dominate the transfer function.

Additionally, while our prior work [8] implemented two interleaved channels per electrode, acquisition of ECG was performed in a single-ended unipolar manner, thereby limiting our ability to add a driven right leg (DRL) circuit and limiting achievable CMRR. In contrast, Chi et al. [10] proposed a differential architecture that averaged the common-mode signal across all acquired channels for increased CMRR.

In this paper, we combine the two-channel interleaved electrode with a differential DRL-compatible architecture that, along with a modified electrode model and improved reconstruction algorithm, enables higher-fidelity recovery of electrode impedance variation compared to our prior work. This paper presents the hardware design of a two-electrode system, detailed frequency-domain analysis of the proposed signal recovery technique, and measurement results indicated up to a 76.3% improvement in non-contact signal acquisition.

978-1-4799-7234-0/15/$31.00 ©2015 IEEE

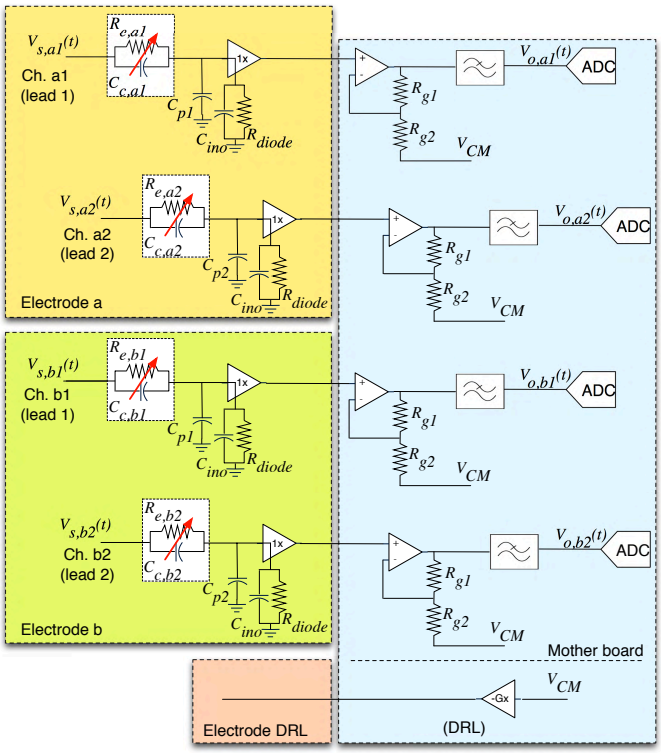

Figure 2. The impedance-compensating non-contact ECG recovery system.

II. ARCHITECTURE

Figure 2 shows the architecture of the impedance-compensating non-contact ECG recovery system together with the electrode model and input parasitic components. In this system, Ch.a1 and b1 form a differential pair across two different electrodes (Lead 1), while Ch.a2 and Ch.b2 form a second differential pair (Lead 2).

The impedance of the first stage must be large in order to minimize impedance divider effects of the input signal, and yet the input must be biased at a DC voltage. Instead of biasing via a very large resistor, which has associated parasitics and would significantly increase the design area, the first stage is instead biased by the employed Op-Amp's own electrostatic discharge protection (ESD) diodes, R_{diode}, which provides a high equivalent resistance, >30GΩ. This resistance, together with the effective input capacitance of the Op-Amp, C_{ino}, and the parasitic board capacitance, C_{p1}, form the total input impedance of each channel. These values are all time-invariant and known a priori at design time or via direct measurement.

On the other hand, the electrode impedance comprising R_e and C_C are unknown and time-variant. Fortunately, the interleaved channels on each electrode are designed such that R_e and C_C are the same for a single electrode. Since the ECG source in the human body model can be modeled as a floating voltage source, the impedance of electrodes a and b and the Z_{in} composed by R_{diode} and C_{ino} will form a Kirchhoff voltage loop as shown in Figure 3. The loop current, I_{loop}, and the voltages $V+$ and $V-$ at the Op-Amp inputs are described by Eq. (2), illustrating that the measured differential voltage depends on both electrode impedances.

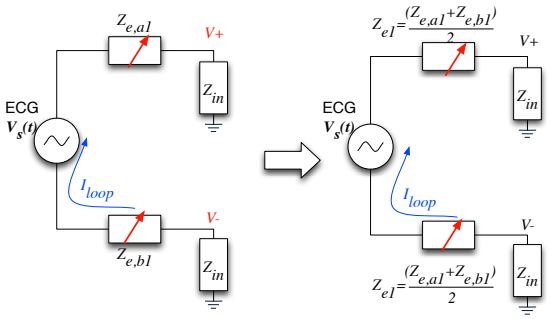

Figure 3. A loop formed by a differential channel pair.

$$\begin{cases} I_{loop} = \dfrac{V_s(t)}{Z_{e,a1}+Z_{e,b1}+2Z_{in}} \\ V+ = I_{loop}Z_{in} = \dfrac{V_s(t)}{2}\dfrac{Z_{in}}{(\frac{Z_{e,a1}+Z_{e,b1}}{2})+Z_{in}} \\ V- = -I_{loop}Z_{in} = -\dfrac{V_s(t)}{2}\dfrac{Z_{in}}{(\frac{Z_{e,a1}+Z_{e,b1}}{2})+Z_{in}} \end{cases}$$

III. DISTORTION DUE TO THE VARIATION OF ELECTRODE IMPEDANCE

In long-term ECG monitoring, both R_e and C_C vary with complex conditions of the intermediate dielectric. For example, respiration can change the pressure between the electrode and the skin, which can change the thickness of the dielectric, thereby changing R_e and C_C, which serve to distort the measured waveform. Similarly, environmental condition such as moisture accumulated from sweat can increase the conductivity of clothes, thereby decreasing R_e. Since the model varies with time and frequency, we will first analyze the transfer function and then propose an equalization scheme.

The transfer function of the electrode-amplifier impedance divider is shown in Eq. (3).

$$H(s) = \frac{Z_e}{Z_{in}+Z_e} = G_h\frac{(s+z_1)}{(s+p_1)}, \tag{3}$$

where $Z_e = R_e \| \frac{1}{sC_C}$, $Z_{in} = R_{diode} \| \frac{1}{s(C_P+C_{ino})}$, $G_h = \frac{C_C}{C_C+C_P+C_{ino}}$, $z_1 = \frac{1}{R_eC_C}$, and $p_1 = \frac{R_e+R_{diode}}{R_eR_{diode}(C_C+C_P+C_{ino})}$.

As illustrated in Fig. 4, the behavior of this transfer function can be considered as an all-pass filter with two flat bands and one transition region between them. We will analyze the effects of magnitude and phase separately.

A. Magnitude

The two flat bands in Fig. 4 are denoted as G_h and G_l for the higher and lower frequency ranges, as derived in Eqns. (3) and (4), respectively. Figure 4 illustrates that the transition takes place between z_1 and p_1 for Lead 1, and z_2 and p_2 for Lead 2, where the slope is 20dB/decade.

$$G_l = \frac{R_{diode}}{R_{diode}+R_e} \tag{4}$$

If the minimum of $z_{\{1,2\}}$ and $p_{\{1,2\}}$ is larger than the lowest frequency of ECG spectrum, then the ECG spectrum will be split into two flat bands and then distorted by two different gains. These two disparate gains distorts the actual ECG signal,

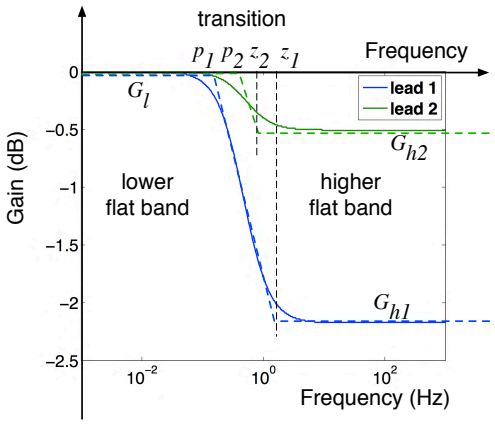

Figure 4. Simulated transfer function (solid) and Bode plot (dashed) of electrode 1 (blue) and 2 (green). Here, the component values are the nominal values in practice, C_{ino} = 20pF, R_{diode} = 30GΩ, C_{p1} = 0pF, C_{p2} = 100pF, R_{e1} = 0.1GΩ, R_{e2} = 0.1GΩ, C_{C1} =150pF, and C_{C2} = 150pF.

$V_s(t)$, and must be corrected for high-fidelity signal capture. To eliminate this distortion, we propose a self-calibrating frequency-domain equalization scheme as described in Section IV.

B. *Phase Difference*

If a circuit presents zero phase difference, there will be no dispersion, i.e. all frequency components of a input signal pass through together. The phase of H(s) is shown in Eq. (5).

$$\angle H(\omega) = arc\tan\left(\frac{\omega(z_1 - p_1)}{-\omega^2 - z_1 p_1}\right) \approx \frac{\omega\left(\frac{R_e(C_p + C_{ino})}{R_e C_C R_e (C_C + C_p + C_{ino})}\right)}{-\omega^2 - \frac{1}{R_e C_C R_e (C_C + C_p + C_{ino})}} \quad (5)$$

Considering practical component values: 20MΩ≤ R_e ≤2GΩ, 20pF≤ C_C ≤400pF, C_{ino} = 20pF and R_{diode} = 30GΩ, the phase change across frequencies of interest is less than 0.1 rad, and thus dispersion effects can be ignored. As a result, we are safe to propose a time-domain recovery method regardless of the tail in the impulse response of the all-pass filter.

IV. Signal Processing

We propose a time-domain signal restoration signal processing algorithm which lowers the requirement for a high resolution in frequency domain to distinguish the three bands illustrated in Fig. 4. Besides, this algorithm leverages the advantage of real-time FIR/IIR filtering, which is linear in complexity, cheaper than FFT and equalization the distortion in frequency domain, O(n *log* n), if implemented in software.

Figure 5 depicts the signal flow diagram of the proposed ECG recovery algorithm. The raw data is first bandpass filtered into M adjacent equal-width frequency bands, $band_m$ where $m \in \{1...M\}$. If the bandwidth of each bandpass filter is small enough, the impedance inside the band is approximately fixed. Thus we can select the center frequency of each band to calculate the input impedance, $Z_{in,m}$, which is synthesized with R_{diode}, C_p and C_{ino} in parallel.

Assuming any baseline drifting can be removed by software de-trending, Eq. (6) is the generalized form of Eq. (1),

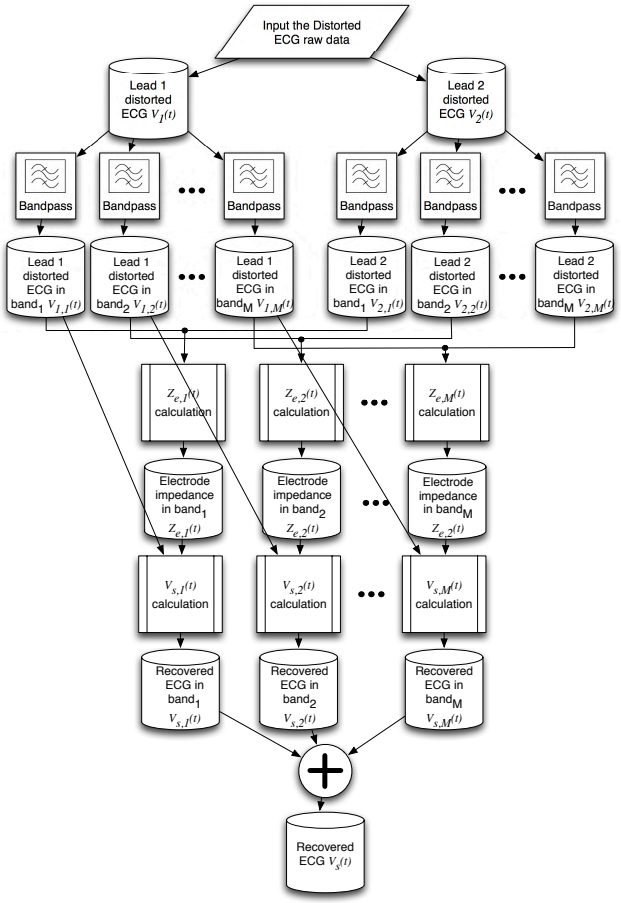

Figure 5. The flow diagram of the signal processing for ECG recovery.

where $Z_{e,m}(t)$ and $V_{s,m}(t)$ represents the electrode impedance and filtered ECG in $band_m$, respectively.

$$\begin{cases} V_{1,m}(t) = \dfrac{V_{s,m}(t) Z_{in1,m}}{Z_{in1,m} + Z_{e,m}(t)} \\ V_{2,m}(t) = \dfrac{V_{s,m}(t) Z_{in2,m}}{Z_{in2,m} + Z_{e,m}(t)} \end{cases} \quad (6)$$

Solving Eq. (6) yields Eq. (7) for each $band_m$, and substituting $Z_{e,m}(t)$ back to Eq. (6) allows us to recover the ECG in $band_m$, $V_{s,m}(t)$.

$$Z_{e,m}(t) = \frac{Z_{in1,m} Z_{in2,m} (V_{2,m}(t) - V_{1,m}(t))}{V_{1,m}(t) Z_{in2,m} - V_{2,m}(t) Z_{in1,m}} \quad (7)$$

The last step is to sum over every $V_{s,m}(t)$ to obtain the recovered ECG.

V. Experimental Results

A series of experiments are taken to verify the proposed ECG recovery system. The employed interdigitated non-contact ECG electrodes are shown in Fig. 6. Each electrode supports two channels that are assigned a slightly different input capacitance. Each non-contact electrode was then placed next to a conventional wet-contact electrode used as a benchmark. For the signal processing, there are 5 band-pass filters implemented in this experiment.

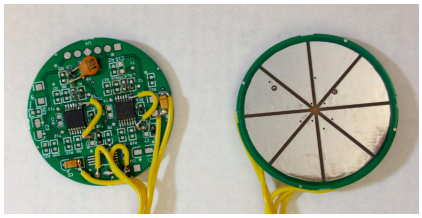

Figure 6. The interdigitated non-contact ECG electrodes. The left one shows top side; the right one bottom. The diameter is 4.2cm.

Measured results taken when a subject was sitting are shown in Fig. 7. Here, it can be seen that the R, and S peaks are significantly distorted in the raw data waveform prior to reconstruction processing. This means the ECG spectrum was split into different bands as predicted. After processing, the recovered ECG matches the wet-contact benchmark very well, decreasing the dissimilarity to the wet-contact ECG by 42.2% from 0.0393 to 0.0227, where the dissimilarity is defined with Pearson correlation as shown in Eq. (8), which normalizes the gain difference between the non-contact and wet-contact ECGs.

$$Dissim = 1 - \frac{\sum_i (x_i - \bar{x})(y_i - \bar{y})}{\|x_i - \bar{x}\|\|y_i - \bar{y}\|} \quad (8)$$

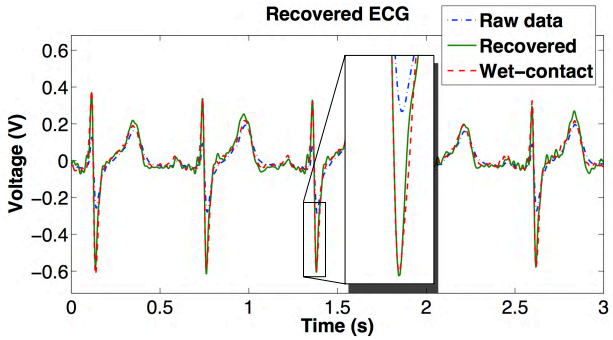

Figure 7. Measured ECG before and after recovery when sitting.

Measured results during an experiment in which the subject was walking are shown in Fig. 8. This case shows the transfer function changes versus time due to motion. Note that motion artifacts at around 1.5s result in serious distortion of the raw non-contact data in comparison to the wet-contact electrode. Fortunately, the impedance-compensating recovery system successfully removes this motion artifact, improving the dissimilarity to the wet-contact ECG by upwards of 76.3% (0.0956 to 0.0226). More results, averaged over 500 PQRST complexes, are listed in Table I.

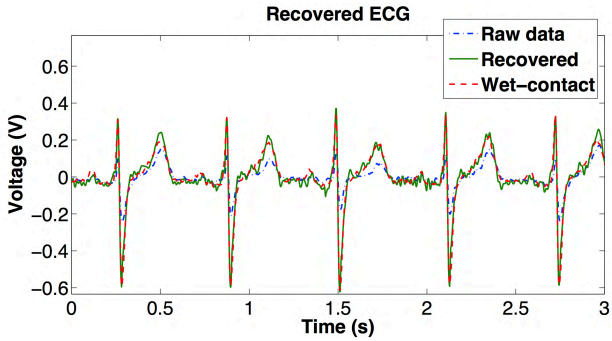

Figure 8. Measured before and after recovery when walking.

	# of trials	Dissim. of raw data			Dissim. of recovered data			Improvement
		min	max	avg	min	max	avg	
Sitting	10	0.0440	0.0489	0.0478	0.0293	0.0319	0.0317	33.6%
Walking	10	0.0467	0.0512	0.0497	0.0350	0.0570	0.0359	27.7%
Running	10	0.0480	0.0530	0.0517	0.0399	0.0430	0.0418	19.2%

TABLE I. Dissimilarities (the window of each trial is 20s).

Due to an un-optimized detrending process that could not completely eliminate baseline drifting, experiments during running did not show as strong of an improvement due to noise and artifacts at low-frequencies. However, the data was, on average, improved by at least 19.2%.

VI. Conclusions

This paper presented an impedance-compensating non-contact ECG recovery system including a new architecture and new signal processing algorithms to more effectively reduce motion artifacts in realistic environments. To improve signal reconstruction performance over our prior work, we presented detailed analysis of a more realistic resistance+capacitance non-contact electrode model to better understand how variation in electrode parameters affects signal integrity. Based on this analysis, we proposed a band-splitting technique that aims to equalize distortions while simultaneously recovering signal content from two independent channels per electrode. A discrete prototype was developed, and measurement results showed the proposed techniques can improve performance compared to raw data capture by upwards of 76.3%.

References

[1] T. Matsuo, K. Iinuma, and M. Esashi, "A barium-titanate-ceramics capacitive-type EEG electrode." *IEEE Trans. Biomedical Engineering*, vol. BME-20, no. 4, pp. 299–300, Jul. 1973.

[2] A. Ueno, Y. Akabane, T. Kato *et al*, "Capacitive sensing of electrocardiographic potential through cloth from the dorsal surface of the body in a supine position: a preliminary study," *IEEE Trans. Biomedical Engineering*, vol. 54, pp. 759-766, 2007.

[3] C. Harland, T. Clark, and R. Prance, "Electric potential probes-new directions in the remote sensing of the human body," *Measurement Science and Technology*, vol. 13, no. 2, p. 163, Feb. 2002.

[4] A. Aleksandrowicz and S. Leonhardt, "Wireless and non-contact ECG measurement system–the 'Aachen SmartChair'," *Acta Polytechnica*, vol. 47, no. 4–5, pp. 68–71, Jun. 2007.

[5] S. Heuer, D. R. Martinez, S. Fuhrhop, and J. Ottenbacher, "Motion artefact correction for capacitive ECG measurement," in *Proc. IEEE Biomedical Circuits and Systems Conf.* (BioCAS), 2009, pp. 113–116.

[6] A. Serteyn, R. Vullings, M. Meftah, and J. W. M. Bergmans, "Motion artifacts in capacitive ECG measurements: reducing the combined effect of DC voltages and capacitance changes using an injection signal," *IEEE Trans. Biomedical Engineering*, vol. 62, no. 1, pp. 264–273, Jan. 2015.

[7] B. Yin, M. Meftah, and T. J. Ikkink, "Compensation of motion artifacts in capacitive measurement of electrophysiological signals," U.S. Patent 20 110 137 200, 2011.

[8] H. Su, H. Liu, S.-H. Weng *et al*, "A non-contact biopotential sensing system with motion artifact suppression," in *Proc. IEEE Int. Conf. Communications, Circuits and Systems* (ICCCAS), 2013, pp. 314–318.

[9] N. Gandhi, C. Khe, D. Chung *et al*, "Properties of dry and non-contact electrodes for wearable physiological sensors," in *Proc. IEEE Int. Conf. Body Sensor Networks* (BSN), 2011, pp. 107–112.

[10] Y. Chi, P. Ng, E. Kang, J. Kang, J. Fang, and G. Cauwenberghs, "Wireless non-contact cardiac and brain monitoring," in *Proc. ACM Wireless Health*, 2010, pp. 15–23.